Surfactant-Free Hydrothermal Synthesis of Highly Tetragonal Barium Titanate Nanowires: A Structural Investigation

ARTICLE *in* THE JOURNAL OF PHYSICAL CHEMISTRY B · JULY 2006

Impact Factor: 3.3 · DOI: 10.1021/jp0600110 · Source: PubMed

4 AUTHORS, INCLUDING:

Songhak Yoon
..
74 PUBLICATIONS **636** CITATIONS
SEE PROFILE

Sunggi Baik
Pohang University of Science and Technology
178 PUBLICATIONS **2,842** CITATIONS
SEE PROFILE

Jason JS Lee
National Yang Ming University
612 PUBLICATIONS **13,169** CITATIONS
SEE PROFILE

Surfactant-Free Hydrothermal Synthesis of Highly Tetragonal Barium Titanate Nanowires: A Structural Investigation

Upendra A. Joshi,[†] Songhak Yoon,[‡] Sunggi Baik,[‡] and Jae Sung Lee*,[†]

Department of Chemical Engineering and School of Environmental Science and Engineering and Department of Materials Science and Engineering, Pohang University of Science and Technology (POSTECH), San 31 Hyoja-dong, Pohang 790-784, Korea

Received: January 2, 2006; In Final Form: April 26, 2006

Barium titanate nanowires synthesized with a surfactant-free hydrothermal method have been characterized by various techniques such as transmission electron microscopy (TEM), scanning electron microscopy (SEM), synchrotron X-ray diffraction, X-ray photoelectron spectroscopy (XPS), and Raman spectroscopy. The TEM and SEM analyses show the uniform cylindrical nanowires. The Rietveld refinement with synchrotron X-ray powder diffraction showed that the lattice parameters of cubic and tetragonal phases were a ($= b = c$) = 4.0134 Å and a ($= b$) = 3.9998 Å, c = 4.0303 Å, respectively. The final weighted R-factor, R_{wp}, was 6.75% and the goodness of fit indicator was 1.30. The mass fraction of tetragonal and cubic phases based on the refined scale factor for the two phases were 98.4% and 1.6%, respectively, which clearly show the nanowires are tetragonal. The XPS analysis has shown that as-obtained $BaTiO_3$ nanowires were phase pure. The Raman spectra confirm the tetragonal phase of the $BaTiO_3$ nanowires. The dielectric constant measurement shows the shift in the transition temperature (T_c = 105 °C) compared to the bulk transition temperature (T_c = 132 °C). The dielectric constant at T_c was 174 measured at 1 kHz frequency.

1. Introduction

Ferroelectronic oxides constitute an important class of multifunctional compounds, attractive for numerous technological applications such as thermisters, multilayer capacitors, and electrooptical devices. Intense experimental efforts have been made recently in synthesizing and understanding ferroelectric (FE) nanostructures—$BaTiO_3$ dots,[1] rods,[2] wires,[3] and nanotubes[4]—mainly because of their promise in increasing FE nonvolatile memory density thousands fold by reading and writing into *individual nanoparticles*.[3,5,6] Furthermore, these structures are also critical in light of miniaturizing piezoelectric transducers and actuators, ultrasonic devices, and medical imaging detectors.[7,8] From a fundamental point of view, ferroelectricity is caused by atomic off-center displacements, resulting from a delicate balance between long-range (LR) Coulomb interaction and short-range (SR) covalent interaction.[9] In nanostructures, both interactions and thus their balance are altered with respect to bulk, since the LR interaction is truncated due to lack of periodicity, while the SR one is significantly modified near the surface boundary.

With decreasing particle size in the $BaTiO_3$ perovskite lattice, an increase in cubic lattice parameter has been observed at room temperature.[10−18] These results are attributed to so-called size-dependent ferroelectric phase transition, which is the room temperature crystal structure transformation from tetragonal (ferroelectric phase) to cubic (paraelectric phase) with decreasing particle size. Moreover, it is reported that cubic barium titanate is stabilized with expanded unit cell due to the existence of hydroxyl ion incorporated in the lattice.[19−21] Depending on the transition temperature, $BaTiO_3$ has four kinds of crystal systems, i.e., rhombohedral, orthorhombic, tetragonal, and cubic. There is an additional hexagonal modification reported by Megrew and Burbank et al.[22,23] Among them, the high-temperature form is the cubic phase and the stable phase at room temperature is the tetragonal phase. Cubic (space group: $Pm\bar{3}m$) $BaTiO_3$ has an ideal perovskite-type structure. The cubic phase transforms into a high-temperature hexagonal structure (space group: $P6_3mmc$) around 1432 °C.[24] A cubic-to-tetragonal structural phase transition occurs around 132 °C. The tetragonal $BaTiO_3$ (space group: $P4mm$) has atomic displacements which exhibit ferroelectricity. This phenomenon implies that the phase transformation of $BaTiO_3$ may be a function of the temperature and the crystallite size. There is a crystallite size that makes it transform from tetragonal to cubic phase at room temperature.[12,25,26] Depending on the synthetic methods there have been various critical sizes, ranging from 25 to 200 nm.[27] To predict the variation of physical properties of $BaTiO_3$ powder with the critical size, it is necessary to determine the critical size of various synthesis methods and to obtain the structural information. However, the dielectric constant of fine particles decreases with decreasing their size.

It is known that the existence of impurities such as lattice hydroxyl ($^-$OH) and carbonate (CO_3^{2-}) groups in $BaTiO_3$ particles considerably decreases the dielectric constant. Recently, Wada et al.[28−30] have succeeded in the preparation of $BaTiO_3$ fine particles with very few lattice hydroxyl groups by means of a two-step thermal decomposition method from barium titanyl oxalate. The dielectric constant of the impurity-free $BaTiO_3$ fine particles increases with their decreasing size in the range from 430 to 140 nm but decreases from 140 to 40 nm.[30]

Hydrothermal synthesis has been widely used for the preparation of the nanostructured materials and shown to be effective in particular for the synthesis of nanowires, nanorods, and

* To whom correspondence should be addressed. Phone: 82-54-279-2266. Fax: 82-54-279-5528. E-mail: jlee@postech.ac.kr.

[†] Department of Chemical Engineering and School of Environmental Science and Engineering.

[‡] Department of Materials Science and Engineering.

10.1021/jp0600110 CCC: $33.50
Published on Web 06/06/2006

nanotubes.[31,32] It has advantages in reducing processing temperature and yielding a nearly site-ordered phase while producing fine crystalline powders. Recently, we reported the template-free hydrothermal synthesis and investigation of the formation mechanism of single-crystalline barium titanate and strontium titanate nanowires.[33] As the structural data including lattice constants, atomic positions, and phase fraction are closely related to the physical properties, here we report the detailed structural characteristics of $BaTiO_3$ nanowires by means of the Rietveld refinement using X-ray powder diffraction data. The Raman spectroscopy and XPS analysis have been performed for the phase identification of $BaTiO_3$ nanowires along with dielectric measurements.

2. Experimental Section

2.1. Synthesis of Materials. All the operations were carried out in a glovebox filled with nitrogen in the absence of moisture or CO_2. CO_2-free water (distilled water boiled for 15 min in a nitrogen atmosphere) was used for all processes. In a typical synthesis, an equimolar amount of $Ba(OH)_2$ and TiO_2 particles (Merck) were mixed together in a mortar pester for 1 h in the presence of ethanol as a solvent. The mixture was taken out of the glovebox and transferred to a Teflon-coated reactor containing water (20 mL) and thereto (20 mL of) liquid ammonia was added to adjust the pH above 13. Then the reactor was put into hydrothermal reaction at a constant temperature (170 °C) without disruption for 3 days. The as-synthesized white precipitate was washed with water and dried in an oven at 60 °C overnight.

2.2. Characterization of Material. The product was characterized by a number of techniques, including scanning electron microscopy (FE-SEM, FEI XL30S), transmission electron microscopy (TEM, Philips CM-20 with an accelerating voltage of 200 kV), field emission high-resolution transmission electron microscopy (FE-HRTEM, JEOL 2100F), and selected area electron diffraction (SAED). The X-ray powder diffraction experiments were carried out on a 8C2 high-resolution powder diffraction (HRPD) beamline at Pohang Light Source (PLS) in Pohang, Korea. The incident X-rays were monochromatized to the wavelength of 1.5492 Å by a double bounce Si (111) monochromator. The flat specimen was rotated in the plane of the specimen surface at 60 rotations/min during the scan to eliminate the influence of preferred orientation. The diffraction pattern was scanned from 15° to 131° (2θ) with a step length of 0.01 and a fixed counting time of 3 s. X-ray diffraction patterns have been fitted by means of a Rietveld refinement program, Fullprof, to determine the crystallite size and tetragonallity (c/a ratio) in the powder. A pseudo-Voigt function was chosen as a profile function among profiles in Fullprof. The composition of $BaTiO_3$ nanowires was determined by X-ray photoelectron spectroscopy (XPS, VG Scientific ESCALAB 220iXL). The spectrometer was equipped with a hemispherical analyzer and all XPS data presented here were acquired with use of Mg Kα as the X-ray source (1253.6 eV). All binding energies of various peaks were calibrated by using the binding energy of C 1s (285.1 eV). Raman spectra of various $BaTiO_3$ nanowires were obtained with a NRS2100 Raman spectrometer (JASCO, Japan) equipped with a triple-grating monochromator and a Coherent Innova 90C Ar^+-laser operating at 514.5 nm with the power of 300 mW. It has a spectral resolution of 1 cm^{-1}. The measurement was performed with a micro-Raman option, using a backscattering configuration. The dielectric constant measurement was performed on $BaTiO_3$ nanowire disks, using a HP 4284A precision LCR meter with the four different frequencies, 1, 10, 100, and 1000 kHz. Silver paste was coated on the disk as an electrode. For the measurement of dielectric constant as a function of temperature, the sample is heated at a rate of 3 deg/min from room temperature to the 200 °C. Fourier Transform Infrared spectra (FT-IR) of as-obtained nanowires were obtained with a FT-IR Instrument (MIDAC Corporation) attached with ICON FT-IR analytical software.

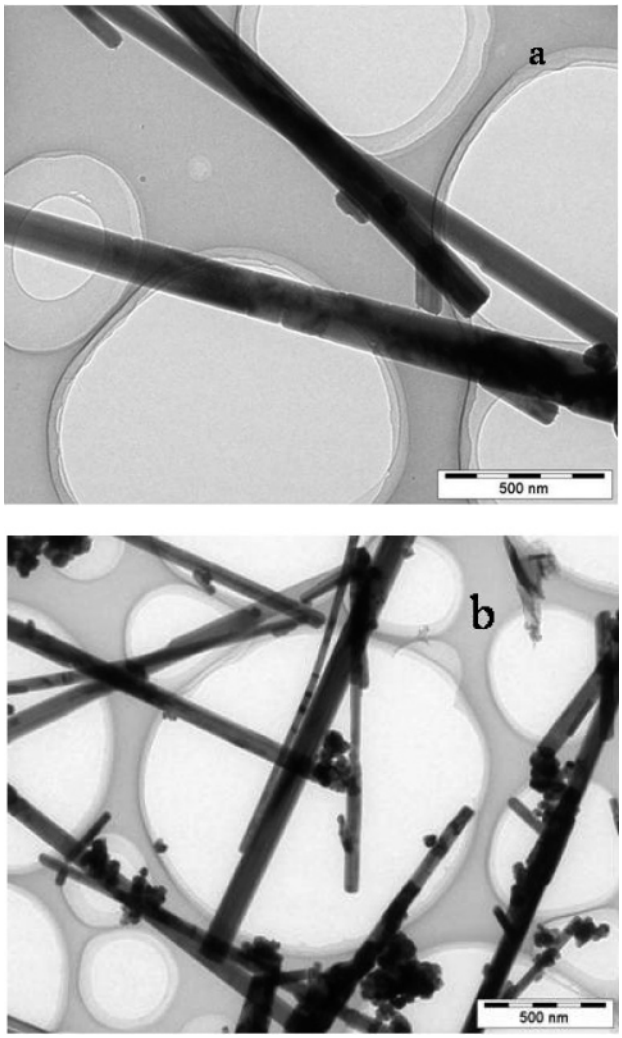

Figure 1. TEM images of $BaTiO_3$ nanowires.

3. Results

A surfactant-free hydrothermal synthetic procedure for $BaTiO_3$ nanowires has been described in detail in our previous publication.[33] Representative transmission electron microscopy (TEM) images of the product obtained by hydrothermal reaction of TiO_2 particles and $Ba(OH)_2$ have been shown in Figure 1. These images clearly show that $BaTiO_3$ nanowires have straight and uniform cylindrical structures with diameters in the range of 50−200 nm and lengths from a few to tens of micrometers. Figure 1b shows several nanowires entangled in each other. These TEM images show that each nanowire has a uniform diameter along with their length. Figure 2 shows the SEM images of as-obtained $BaTiO_3$ nanowires. From Figure 2a it is clear that the $BaTiO_3$ nanowires are of a straight and cylindrical structure with diameter of about 50 nm and lengths of several micrometers. The inset of Figure 2a shows the tip of a nanowire, which clearly exhibits the circular cross section of the nanowires. Figure 2b shows a single $BaTiO_3$ nanowire. It is observed from 30 different samples that the as-synthesized product contained about ca. 90% nanowires and about ca. 10% nanoparticle aggregated.

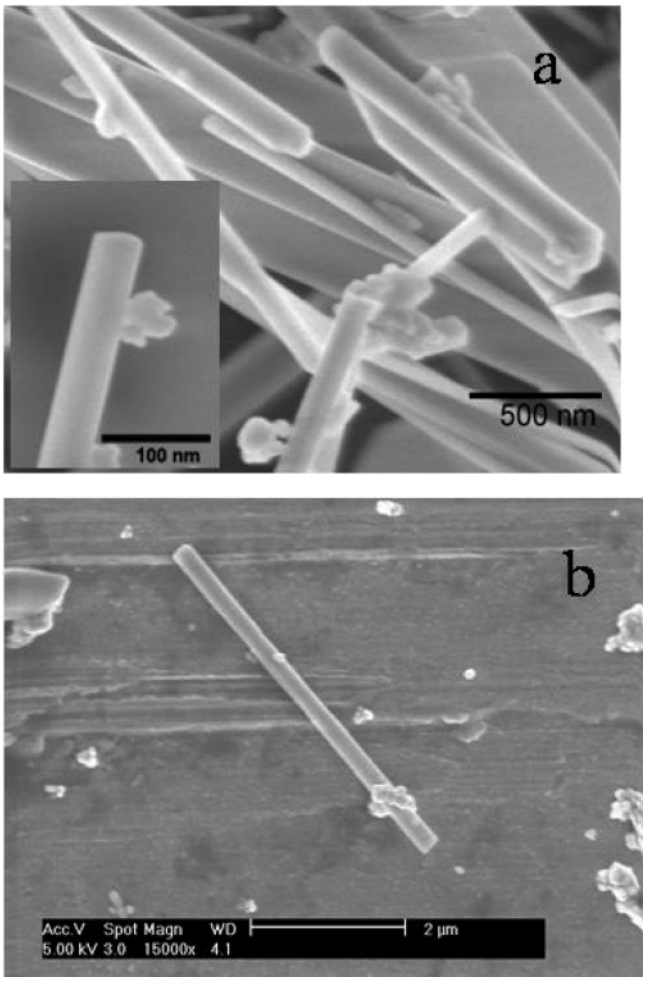

Figure 2. SEM images of $BaTiO_3$ nanowires.

The evidence for the formation of single-crystalline $BaTiO_3$ nanowires could be found in high-resolution TEM (HR-TEM) image (Figure 3a) and selected area electron diffraction (SAED) patterns along the [001] zone axis shown in Figure 3b. Figure 3a shows the lattice fringes of $BaTiO_3$ nanowires. On the basis of the calculations of the lattice spacing and the analysis of its orientation, it was found that the nanowires grow perpendicular to [110]. The HR-TEM images of $BaTiO_3$ nanowires reveal that the surfaces of the nanowires are clean, very regular, and without any sheath of amorphous phase. This further confirms the single-crystalline nature of these nanowires. The SAED pattern in Figure 3b shows the sharp diffraction spots of (010) and (100) planes, which is characteristics of crystalline $BaTiO_3$. Furthermore, the SAED patterns taken from different nanowires are identical, indicating that the nanowires are single crystals.

Figure 4 shows the Rietveld refinement patterns of as-synthesized $BaTiO_3$ nanowires with use of the cubic and tetragonal phase model. The inset in Figure 4 shows a close-up of the higher angle region. The least-squares fit of the pattern with use of the *P*4*mm* and $Pm\bar{3}m$ symmetries in Fullprof yielded the structure parameters summarized in Table 1. The Rietveld refinement reveals that the structure model with two phases of the cubic and tetragonal components gives the best fit for the XRD pattern compared to the cubic phase or tetragonal phase alone. The lattice constants for $BaTiO_3$ have been determined to be $a = 4.0134$ Å for cubic phase and $a = 3.9998$ Å and $c = 4.0303$ Å for tetragonal phase, which is in agreement with those for the corresponding bulk tetragonal materials ($a = 3.9947$ Å and $c = 4.0336$ Å at room temperature).[34] Figure 5 shows the

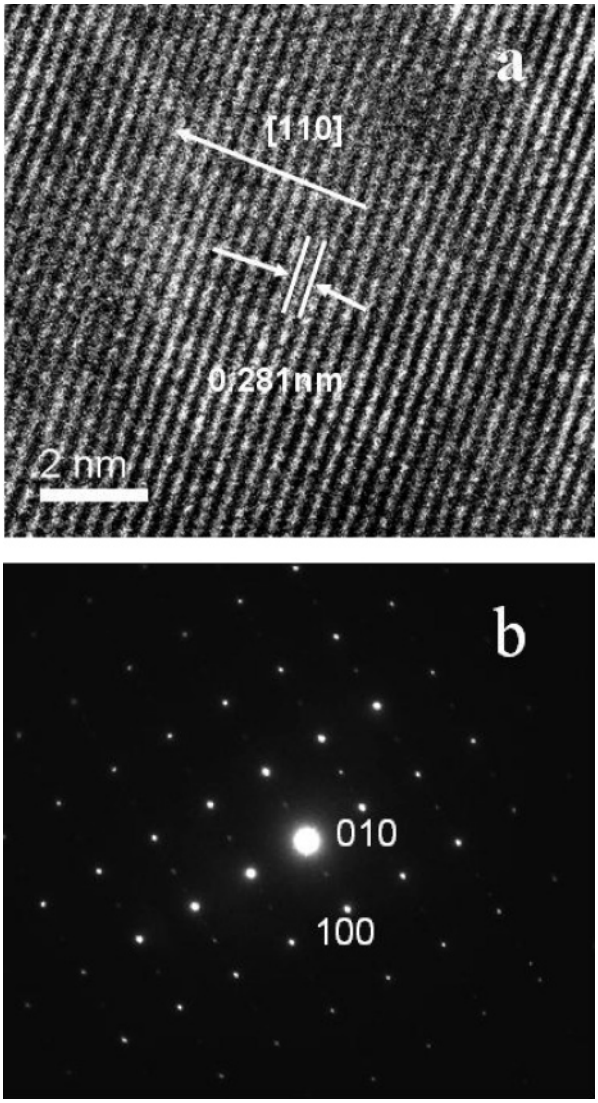

Figure 3. (a) HR-TEM image of $BaTiO_3$ nanowire and (b) selected area diffraction pattern of $BaTiO_3$ nanowire.

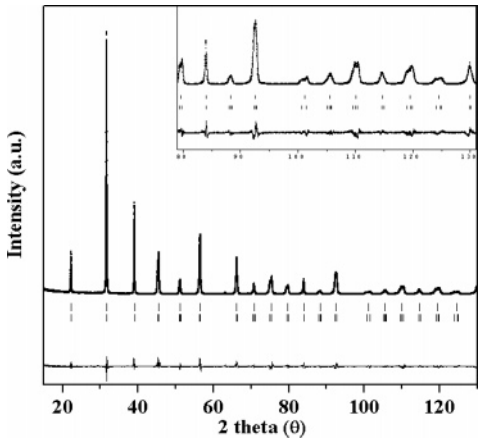

Figure 4. Powder X-ray diffraction data and calculated diffraction profiles from the Rietveld refinement of the tetragonal phases of $BaTiO_3$. The difference plots of observed and calculated diffraction profiles are shown below, and the short vertical markers represent the peak positions. The inset shows a close-up of the higher angle region.

results of the Rietveld refinement for the data of $BaTiO_3$ nanowires, assuming three models: (a) cubic structure model, (b) tetragonal structure model, and (c) composite structure model with cubic and tetragonal components. Figure 6a,b shows the

TABLE 1: Refined Crystal Parameters and Reliability Factors of $BaTiO_3$ Nanowires[a,b]

	atom	X	Y	Z	U (10^{-2} Å)
tetragonal	Ba	0.000	0.000	0.000	0.61379
*P*4*mm*	Ti	0.500	0.500	0.475(5)	1.17987
$a = 3.99984$	O1	0.500	0.500	0.029(1)	1.26313
$c = 4.03033$	O2	0.500	0.000	0.528(2)	0.21346
	atom	X	Y	Z	U (10^{-2} Å)
cubic	Ba	0.000	0.000	0.000	2.57748
$Pm\bar{3}m$	Ti	0.500	0.500	0.500	0.89665
$a = 4.0134$	O1	0.500	0.500	0.000	1.53080

[a] Weight fractions of tetragonal and cubic phases in $BaTiO_3$ nanowires are estimated to be 0.984 and 0.016, respectively. [b] $R_{wp} = 6.75\%$, $\chi^2 = 1.30$ (R_{wp}: reliability factors; χ^2: goodness of fit; U: isotropic thermal factors).

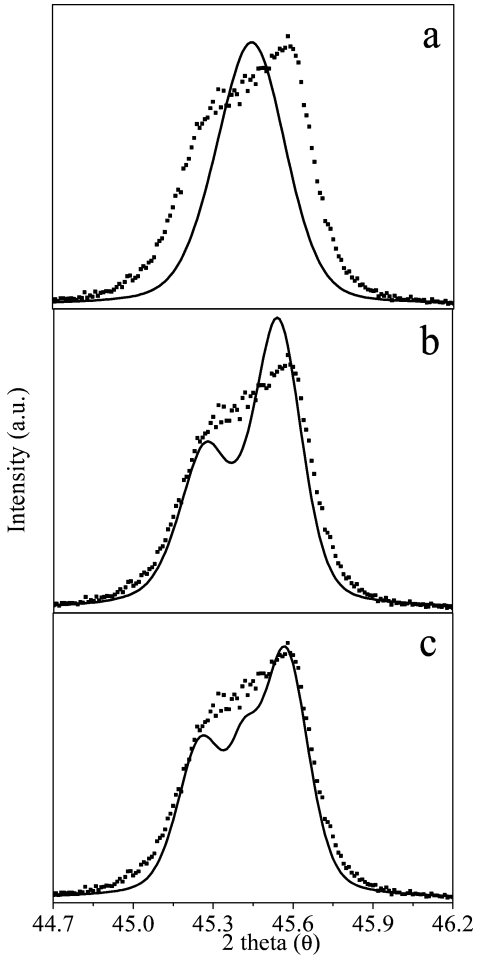

Figure 5. X-ray diffraction data for the {200} reflections dots and results of the Rietveld refinement (lines) for the data of $BaTiO_3$ nanowires, assuming three models: (a) cubic structure model, (b) tetragonal structure model, and (c) composite structure model with cubic and tetragonal components.

cubic and tetragonal crystal structure of $BaTiO_3$ drown with use of refined crystal parameters. The green, light blue, and red spheres denote Ba, Ti, and O atoms, respectively. The tetragonal $BaTiO_3$ (space group: *P*4*mm*) has atomic displacements for Ti and O atoms as shown by the arrows in Figure 6b and exhibits ferroelectricity. The solid line denotes the unit cell.

Figure 7a shows the survey scan XPS spectra of $BaTiO_3$ nanowires. Figure 7b,c shows a deconvolution of spectra fitted with Gaussian shaped curves of Ba $3d^{5/2}$ and Ti $2p^{3/2}$, respectively. Representative Raman spectra of $BaTiO_3$ nanowires have been shown in Figure 8. The tetragonality of $BaTiO_3$ was

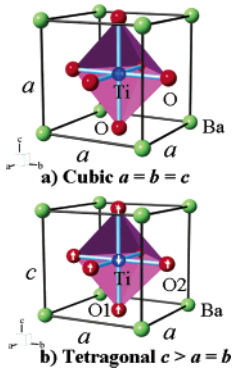

Figure 6. Crystal structures of (a) cubic and (b) tetragonal $BaTiO_3$ drawn by using refined crystal parameters. The green, light blue and red spheres denote Ba, Ti, and O atoms, respectively. The arrows in part b denote the direction of displacements for Ti and O atoms with respect to the Ba atom. The solid line denotes the unit cell.

characterized by two peaks of 307 and 715 cm^{-1}. As our $BaTiO_3$ nanowires clearly show the peaks around 307 and 715 cm^{-1}, it contains a large fraction of the tetragonal structure. To understand the dielectric properties of these $BaTiO_3$ nanowires, we carried out the dielectric measurement. Figure 9 shows the dielectric constant against the measuring temperature of $BaTiO_3$ ceramic disk with different frequency. The ferroelectric transition temperature (T_c) determined by the dielectric maximum is 105 °C. The dielectric constant shows considerable dispersion with frequency change. At low frequency the dielectric constant is high, and as the frequency increases, the dielectric constant decreases. This represents the behavior of a typical dielectric material. To investigate the presence of lattice hydroxyl groups we carried out FT-IR spectroscopy analysis. Figure 10 shows the typical FT-IR spectrum of the as-obtained sample. It is evident that the sample shows the −OH stretching mode indicated by peaks at ∼3500 and ∼1640 cm^{-1}.

4. Discussions

The TEM images in Figure 1 and SEM images in Figure 2 clearly show that the nanowires are straight and without any branching. The confirmation for the single-crystalline nature of $BaTiO_3$ nanowires can be given by HR-TEM and SAED patterns. The Rietveld refinement requires a structural model that has an approximation for the actual structure. The least-squares fit of the pattern with use of the *P*4*mm* and $Pm\bar{3}m$ symmetries in Fullprof yielded the structural parameters summarized in Table 1. The initial Rietveld refinement was done by the zero-point shift, the unit-cell, and background parameters. After a good match in the peak position was achieved, the peak profile parameters including the peak asymmetry were refined. Figure 4 shows the Rietveld refinement patterns of as-synthesized $BaTiO_3$ nanowires, using the cubic and tetragonal phase models. The Rietveld refinement reveals that the structure model with a two-phase model of cubic and tetragonal components gives the best fit for the XRD patters compared to the cubic phase or tetragonal phase model alone. The final weighted *R*-factor R_{wp} of the tetragonal phase model was considerably decreased from 8.42% to 6.75% compared to that of cubic. The profile factor R_p was 4.63%. The indicator for goodness of fit indicator, χ^2, was decreased from 1.74 to 1.34. When we use the two-phase cubic and tetragonal models, the χ^2 value was 1.30, which is lower than that of the single tetragonal phase model and the weight percents of the tetragonal and cubic phase were 98.4% and 1.6%, respectively.

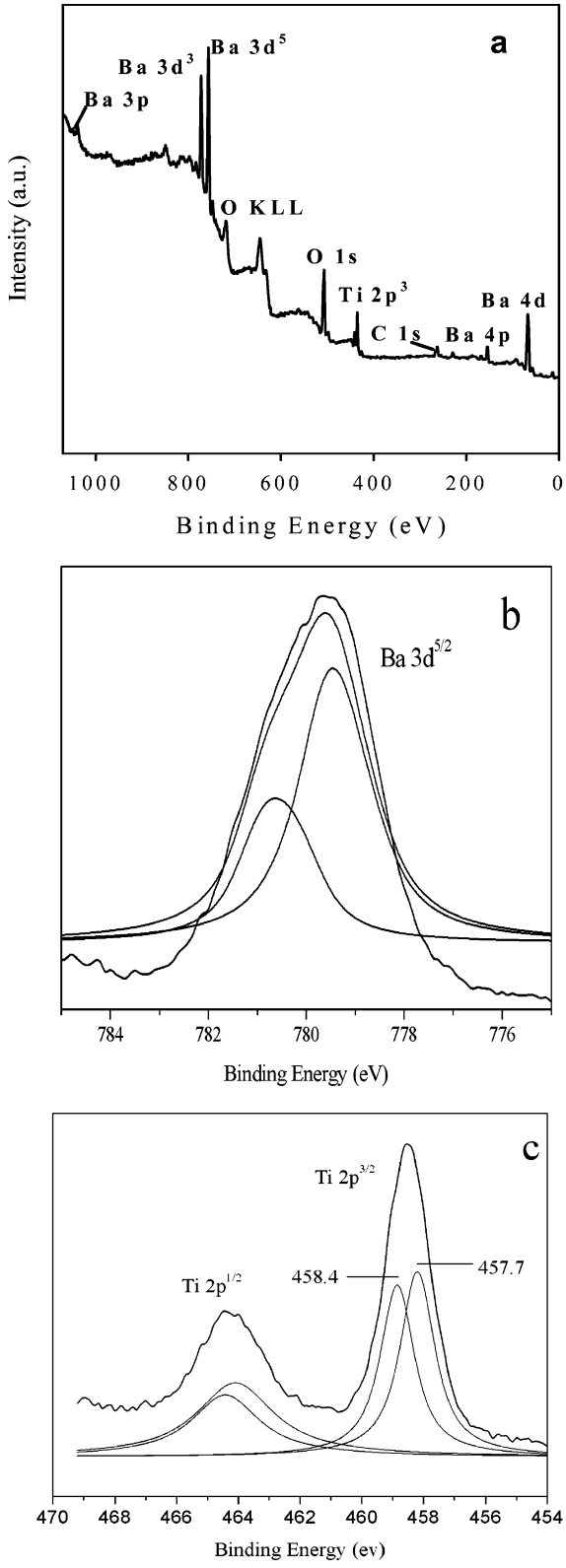

Figure 7. (a) Survey scan XPS spectra of $BaTiO_3$ nanowires, (b) Ba $3d^{5/2}$ spectra, and (c) Ti $2p^{3/2}$ spectra.

The tetragonal phase has two peaks, (002) and (200), which are clearly separated near $2\theta = 45°$, while only the (200) peak of the cubic phase lies between two tetragonal peaks. However, if the size of the crystallite decreases, the two separated peaks of the tetragonal phase may overlap because of the broadening of diffraction peaks. Figure 5 shows the results of the Rietveld refinement for the data of $BaTiO_3$ nanowires assuming three models (a) cubic, (b) tetragonal, and (c) composite structure model with cubic and tetragonal components. Among these three models, the composite structure model with cubic and tetragonal components, as shown in Figure 5c, gives the best fit. From the Rietveld refinement results, it could be concluded that as-synthesized $BaTiO_3$ nanowires have mostly the tetragonal structure with a small portion of the cubic phase. We believe

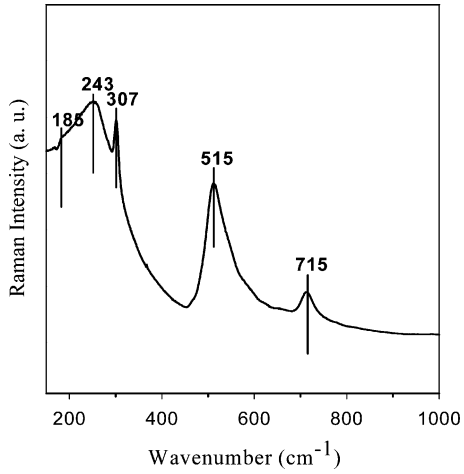

Figure 8. Raman spectra of $BaTiO_3$ nanowires.

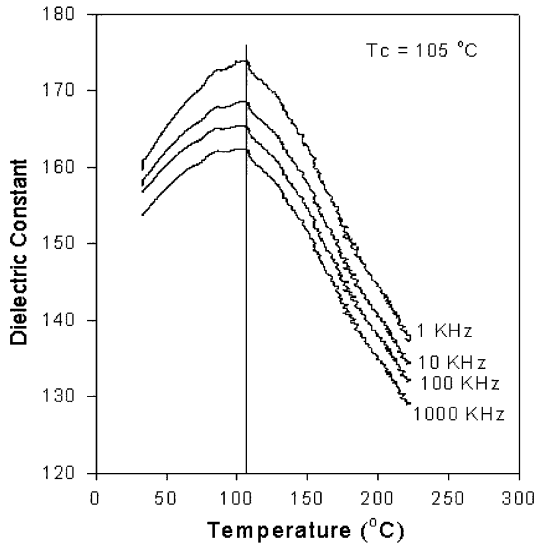

Figure 9. Dielectric constant as a function of measuring temperature at various frequencies for $BaTiO_3$ nanowires disk.

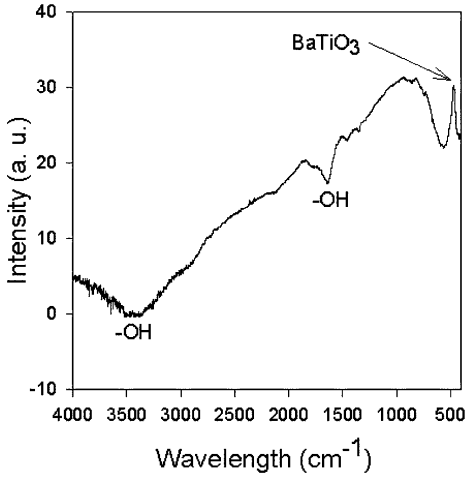

Figure 10. FT-IR spectrum of as-obtained sample: peaks at ~3500 and ~1640 cm^{-1} show the −OH stretching mode.

that a small portion of the cubic structure originated from nanoparticles as the product contains a major portion of nanowires (ca. 90%) and a small portion is made of particles (ca. 10%). As the HRTEM and SAED pattern demonstrate that the nanowires are single crystalline without any sheath of amorphous phase, it is reasonable that the major reflection is of tetragonal phase from nanowires whereas the minor reflection is of cubic phase from nanoparticles.

Considering the structural refinement results for cubic and tetragonal phases, the $BaTiO_3$ nanowires sample shows a major tetragonal phase. Yet, because their crystallite size is small enough, the X-ray diffraction peaks should have been broadened and it is difficult to perform the quantitative analysis with only X-ray diffraction data. Raman spectroscopy and XPS analysis as supplementary methods were chosen to identify the phase and purity of materials, respectively.

We performed XPS studies in order to observe the oxidation state of the metal ions in the sample. Figure 7a shows the survey scan spectra of $BaTiO_3$ nanowires. Panels b and c of Figure 7 show a deconvolution of spectra fitted with Gaussian shaped curves of Ba $3d^{5/2}$ and Ti $2p^{3/2}$, respectively. Two chemical states of Ba can be found: 779.6 eV is assigned to the Ba in the $BaTiO_3$, while the higher energy at 781.2 eV is postulated as a Ba atom linked with the surface hydroxyl group. The binding energy of Ti $2p^{3/2}$ is mainly located at 458.4 and 457.7 eV. The former is consistent with that of $BaTiO_3$ and the latter can be interpreted as low valence Ti^{3+} due to surface oxygen deficiency, which was also observed by other researchers.[35,36] The formation of oxygen and/or barium vacancies must be accompanied by a change in the state of oxidation of the nearest-neighbor Ti atoms from Ti^{4+} to Ti^{3+}, to retain the local charge balance. The above results suggest that the planar defects can be formed due to the complex phenomena associated with Ti^{3+} and oxygen and/or barium vacancies.

Raman scattering has been utilized as a powerful tool to investigate the tetragonal−cubic phase transition.[37] In fact, Raman spectroscopy is a highly sensitive spectroscopic technique to probe the local structure of atoms in the materials. On the basis of the crystallography, only infrared active bonds without first-order Raman activity are predicted for cubic $BaTiO_3$ with a space group of $Pm\bar{3}m$.[37,38] However, eight Raman-active modes are expected for tetragonal $BaTiO_3$ with a space group of $P4mm$.[37] Therefore, only the tetragonal phase will show active vibration mode while the cubic phase will not show any active vibration modes. Room temperature Raman spectra of as-synthesized $BaTiO_3$ nanowires closely agree with those reported in the literature for tetragonal $BaTiO_3$ nanopowder[37,39] and show peaks nearly coincident with those of fundamental modes detected by Raman spectroscopy of tetragonal $BaTiO_3$ nanocrystals.[40]

The $BaTiO_3$ having the cubic symmetry has 15 degrees of freedom for vibration, which are composed of one F_{1u} triply degenerate acoustic mode and three F_{1u} plus one F_{2u} triply degenerate optical modes.[41] In the tetragonal phase, the F_{1u} mode split into three A_1 plus three E modes, and the F_{2u} mode split into B_1 plus an E mode due to the polarization between titanium and oxygen ions, while in the cubic phase neither the F_{1u} nor the F_{2u} mode is active. The four optical E modes for the tetragonal phase are doubly degenerate, which has the polarization along the *x*-axis and the *y*-axis, and the three optical A_1 modes are polarized along the *z*-axis. The E and A_1 modes are split into longitudinal (LO) and transverse (TO) components due to the long-range electrostatic forces associated with lattice ionicity.[42−44,37] In Figure 8, the peaks at 515, 243, and 185 cm^{-1} are assigned to the fundamental TO mode of A_1 symmetry, the peak at 307 cm^{-1} to the B_1 mode indicating asymmetry within the TiO_6 octahedra of $BaTiO_3$ on a local scale. The weak peak around 715 cm^{-1} is related to the highest frequency longitudinal optical mode (LO) with A_1 symmetry. These are typical peaks in the Raman spectrum for the tetragonal $BaTiO_3$ phase. If a peak at 307 cm^{-1} is reduced in its sharpness and becomes indistinct then the tetragonal phase is not dominant. The strong peak at 307 cm^{-1} suggests that the tetragonal phase is dominant in the as-synthesized $BaTiO_3$ nanowires. In addition, sharp peaks at 185, 515, and 715 cm^{-1} indicate the formation of the tetragonal phase. Among these peaks, the peaks around 305 and 715 cm^{-1} disappear above the Curie temperature. This is the stable region for the cubic phase. This means that it is possible to discern between the cubic and tetragonal phases by the presence of the two peaks in the Raman spectrum. It is known that the Raman spectra of both tetragonal and orthorhombic phases of $BaTiO_3$ are similar.[45] The major difference, other than the difference in peak positions, is the appearance of a strong peak around 190 cm^{-1} in the orthorhombic phase instead of the negative peak around 180 cm^{-1} in the tetragonal phase.[45] This is mainly due to the decoupling of the three A_1 (TO) modes in the orthorhombic phase. The presence of asymmetry in the 515 cm^{-1} peak in Figure 8 suggests the presence of coupling of TO modes associated with the tetragonal phase.

This along with the absence of a peak at 190 cm^{-1} proves that our $BaTiO_3$ nanowires have the tetragonal phase, not orthorhombic. These data are consistent with the XRD analysis. A study made by Cho[39] reports the tetragonal structure of $BaTiO_3$ particles 20 nm in size and supports our investigation. There have been several other reports on the critical size of the cubic-to-tetragonal transition and a variety of sizes have been proposed[10,27,43,] ranging from 30 to 100 nm. However, most of these reports involved the use of only powder XRD to analyze the grain size. Theoretical studies with use of the Ginsburg−Landau mean field approach were used earlier[15] to estimate the critical size (44 nm) for the cubic-to-tetragonal phase transition in $BaTiO_3$. Our study shows that the desired tetragonal phase dominantly exists in the $BaTiO_3$ nanowires prepared in the present work. Furthermore the synthetic method used here is simple, but versatile as we do not use any surfactant or template. As the nanowires obtained by the surfactant-free, hydrothermal method show high tetragonality, it should have a relatively high dielectric constant. Hence it could be used for the advancement of the device miniaturization and fabrication.

Figure 9 shows the dielectric constant against the measuring temperature of $BaTiO_3$ ceramic disk with different frequency. The temperature of dielectric maximum obtained by various frequencies is lower (105 °C) than the bulk material (132 °C). This sift may be due to the defects in the crystal or the residual stresses. In the literature this shift is assigned to the size effect mainly due to long-range interaction between electric dipoles[46,47] but some authors also assigned it to stress.[48,49] As such the dielectric constants of as-obtained nanowires are low (174 at T_c and 1 kHz), and there are many causes for size effects in ferroelectrics and it is often difficult to separate true size effects from other factors that change with the size of the sample. For instance, the extreme spreading of the results reported in the literature about the size effect in ferroelectric particles is associated with the variety of synthesis routes and processing techniques adopted.[50] The stability of the ferroelectric phase can be determined by additional factors such as defect chemistry, incorporation of foreign atoms and bulk hydroxyl groups, aggregation level of the particles, porosity level, residual

stresses, etc., as these factors depends on synthesis routes. Generally, in ferroelectrics the boundary conditions can give a strong influence on the stability of the polar phase and on the nature of the size effect.[51,52] Because of the large electrostrictive coupling between spontaneous lattice strain and polarization, the elastic boundary conditions must be considered. Compressive or tensile stresses are expected to change the transition temperature of ferroelectrics. Gupta[48] correlate the effect of stress and particle size. They studied temperature-dependent Raman spectra for sol−gel synthesized thin films (20, 60, 120, 160, 200 nm) above and below the tetragonal−cubic phase transformation. Their conclusion shows that decrease in ferroelectric transition temperature is due to stress but not due to particle size effect.

It is well-known that hydroxyl ions can reside as defects on oxygen sites within $BaTiO_3$ and the resulting charged defects are probably compensated for by cation vacancies.[53,54] Several spectroscopic studies have been carried out to characterize this defect.[55−57] Several authors have reported that infrared spectra for hydrothermally prepared $BaTiO_3$ powders can be interpreted in terms of the presence of internal hydroxyls.[19,58,59] As a result, an intense peak is observed near 3500 cm^{-1} in the IR spectrum. This peak is weak in the case of the Raman spectrum. The possibility that the charged defects might serve to stabilize polar domains in chemically prepared ferroelectric specimens of small crystalline size should also be considered. For fine hydrothermally prepared $BaTiO_3$ powders, other authors have attempted to separate the effect of hydroxyl defects and crystallite size on lattice structure. For instance, Hennings and Schreinemacher[19] clearly showed that the development of a room temperature global tetragonal structure with heat treatment for $BaTiO_3$ nanoparticles of 200 nm diameter, and prepared under hydrothermal conditions from acetate precursors, was associated with the elimination of hydroxyl defect, and not with particle growth. In contrast, Begg, Vance, and Nowotny[12] concluded for hydrothermal powders prepared from $Ba(OH)_2$ and hydrolyzed titanium alkoxide that the release of water from the particles on heat treatment was not at all associated with the development of a tetragonal distortion observed by XRD. Recently, Spanier et al.[60] studied the ferroelectric phase transition in individual single-crystalline $BaTiO_3$ nanowires using scanning probe microscope (SPM) and density functional theory (DFT) calculations. Their study showed that as the diameter of the nanowires decreases the transition temperature (T_c) decreases. The diameter at which T_c falls below room temperature is determined to be ∼3 nm. The DFT calculation indicates that ferroelectricity in nanowires is stabilized by molecular adsorbates such as OH and carboxylates, which is confirmed by FT-IR. In case of our $BaTiO_3$ nanowires study, we essentially observed a similar decrease in transition temperature (T_c = 105 °C); furthermore, the FT-IR spectrum (Figure 10) also shows similar an −OH stretching mode at ∼3500 and ∼1640 cm^{-1} observed by Hennings et al.,[19] Begg et al.,[12] and Spanier et al.,[60] indicating that the samples contain hydroxyl groups. Finally, our study shows that the as-obtained nanowires are highly tetragonal. A ferroelectric study shows the shift in transition temperature (T_c) due to the nanosize effect in the nanowires.

5. Conclusions

The $BaTiO_3$ nanowires have been successfully synthesized via a surfactant-free hydrothermal process. The detailed structural characterization of as-synthesized $BaTiO_3$ nanowires has been carried out by means of the Rietveld refinement, using X-ray powder diffraction, TEM, HR-TEM, SEM, Raman spectroscopy, and XPS analysis. The TEM and SEM analyses show that the nanowires have uniform cylindrical structure with diameters of 50−200 nm and lengths from a few to tens of micrometers. The HR-TEM images of $BaTiO_3$ nanowires reveal that the surfaces of nanowires are clean, very regular, and without any sheath of amorphous phase. The Rietveld refinement with use of X-ray powder diffraction results shows that the $BaTiO_3$ nanowires are made of a mixture of tetragonal (the major) and cubic phases. The mass fraction of tetragonal and cubic phases based on the refined scale factor for the two phases was 98.4% and 1.6%, respectively. The lattice constants for $BaTiO_3$ nanowires were determined as a = 4.0134 Å for the cubic phase and a = 3.9998 Å and c = 4.0303 Å for the tetragonal phase. Further evidence for the presence of the tetragonal phase in the sample could be found in Raman analysis. The sharp peaks at 185, 307, 515, and 715 cm^{-1} signify the tetragonal phase. The phase purity of as-synthesized $BaTiO_3$ nanowires has been confirmed by XPS analysis. From the study of structural characterization it can be concluded that the $BaTiO_3$ nanowires synthesized by the surfactant-free hydrothermal process show high tetragonality. But as we synthesized the nanowires by using ammonia, hydroxyl impurities are incorporated. The presence of the hydroxyl ion is clearly evident from the FT-IR spectrum. The ferroelectric study shows that the transition temperature shifted to the lower values because of the size effect.

Acknowledgment. This work has been supported by the National Research Laboratories Program. We appreciate the support of the Korea Ministry of Education and Human Resources Development through the BK 21 program. U.A.J. thanks Mr. Moongi Jeong and Mr. Young Kyu Jung of the Material Science Department for dielectric measurements and Dr. Namsoo Shin, 8C2 beam line of PAL, for helpful discussions.

References and Notes

(1) O'Brien, S.; Brus, L.; Murray, C. B. *J. Am. Chem. Soc.* **2001**, *123*, 12085.
(2) Urban, J. J.; Yun, W. S.; Gu, Q.; Park, H. *J. Am. Chem. Soc.* **2002**, *124*, 1186.
(3) Yun, W. S.; Urban, J. J.; Gu, Q.; Park, H. *Nano Lett.* **2002**, *2*, 447.
(4) Luo, Y. *Appl. Phys. Lett.* **2003**, *83*, 440.
(5) Scott, J. F.; Paz de Araujo, C. A. *Science* **1989**, *246*, 1400.
(6) Auciello, O.; Scott, J. F.; Ramesh, R. *Phys. Today* **1998**, *51*, 22.
(7) Lines, M. E.; Glass, A. M. *Principles and Applications of Ferroelectrics and Related Materials*; Clarendon: Oxford, UK, 1979.
(8) Uchino, K. *Piezoelectric Actuators and Ultrasonic Motors*; Kluwer Academic: Boston, MA, 1996.
(9) Cohen, R. E. *Nature* **1992**, *358*, 136.
(10) Uchino, K.; Sadanaga, E.; Hirose, T. *J. Am. Ceram. Soc.* **1989**, *72*, 1555.
(11) Schlang, S.; Eicke, H. F. *Solid State Commun.* **1994**, *91*, 883.
(12) Begg, B. D.; Vance, E. R.; Nowotny, J. *J. Am. Ceram. Soc.* **1994**, *77*, 3186.
(13) McCauley, D.; Newnham, R. E.; Randall, C. A. *J. Am. Ceram. Soc.* **1998**, *81*, 979.
(14) Suzuki, K.; Kijima, K. *J. Mater. Sci.* **2005**, *40*, 1289.
(15) Wang, Y. G.; Zhong, W. L.; Zhang, P. L. *Solid State Commun.* **1994**, *90*, 329.
(16) Akdogan, E. K.; Safari, A. *Jpn. J. Appl. Phys.* **2002**, *41*, 7170.
(17) Tsunekawa, S.; Ishikawa, K.; Li, Z.-Q.; Kawazoe, Y.; Kasuya, A. *Phys. Rev. Lett.* **2000**, *85*, 3440.
(18) Tsunekawa, S.; Ito, S.; Mori, T.; Ishikawa, K.; Li, Z.-Q.; Kawazoe, Y. *Phys. Rev. B* **2000**, *62*, 3065.
(19) Hennings, D.; Schreinemacher, S. *J. Euro. Ceram. Soc.* **1992**, *9*, 41.
(20) Noma, T.; Wada, S.; Yano, M.; Suzuki, T. *J. Appl. Phys.* **1996**, *80*, 5223.
(21) Shi, E. W.; Xia, C. T.; Zhong, W. E.; Wang, B. G.; Feng, C. D. *J. Am. Ceram. Soc.* **1997**, *80*, 1567.
(22) Megaw, H. D. *Proc. Phys. Soc.* **1946**, *58*, 133.

(23) Burbank, R. D.; Evans, H. T., Jr. *Acta Crystallogr.* **1948**, *1*, 330.
(24) Kirby, K. W.; Wechsier, B. A. *J. Am. Ceram. Soc.* **1991**, *74*, 1841.
(25) Yamamoto, T.; Urabe, K.; Banno, H. *Jpn. J. Appl. Phys.* **1993**, *32*, 4272.
(26) Li, X.; Shin, W.-H. *J. Am. Ceram. Soc.* **1997**, *80*, 2844.
(27) Yen, F. S.; Hasing, H. I.; Chang, Y. H. *Jpn. J. Appl. Phys.* **1995**, *34*, 6149.
(28) Wada, S.; Narahara, M.; Hoshina, T.; Kakemoto, H.; Tsurumi, T. *J. Mater. Sci.* **2003**, *38*, 2655.
(29) Wada. S.; Yasuno, H.; Hoshina, T.; Nam, S.-M.; Kakemoto, H.; Tsurumi, T. *Jpn. J. Appl. Phys.* **2003**, *42*, 6188.
(30) Wada. S.; Hoshina, T.; Yasuno, H.; Nam, S.-M.; Kakemoto, H.; Tsurumi, T.; Yashima, M. Developments in Dielectric Materials and Electronic Devices. In *Ceram. Trans.* **2005**, *167*, 189.
(31) Vayssieres, L. *Int. J. Nanotechnol.* **2004**, *1*, 1.
(32) Rao, C. N. R.; Deepak, F. L.; Gundiah, G.; Govindaraj, A. *Proc. Solid State Chem.* **2003**, *31*, 5.
(33) Joshi, U. A.; Lee, J. S. *Small* **2005**, *1*, 1172.
(34) Jona, F.; Shirane, G. *Ferroelectric Crystal*; Pergamon: New York, 1962.
(35) Hagendorf, C.; Schindler, K. M.; Doege, T.; Neddermeyer, H. *Surf. Sci.* **1998**, *581*, 402.
(36) Tanaka, H.; Matsumoto, T.; Kawai, T.; Kawai, S. *Surf. Sci.* **1994**, *29*, 318.
(37) Asiaie, R.; Zhu, W.; Akbar, S. A.; Dutta, P. K. *Chem. Mater.* **1996**, *8*, 226.
(38) Didomenico, M., Jr.; Wemple, S. H.; Porto, S. P. S.; Bauman, R. P. *Phys. Rev.* **1968**, *174*, 522.
(39) Cho, W. S. *J. Phys. Chem.* **1955**, *59*, 659.
(40) Chaves, A.; Katiyan, R. S.; Porto, S. P. S. *Phys. Rev. B* **1974**, *10*, 3522.
(41) Scalabrin, A.; Chaves, A. S.; Shim, D. S.; Porto, S. P. S. *Phys. State Sol.* **1997**, *79*, 731.
(42) Dobal, P. S.; Dixit, A.; Katiyar, R. S.; Yu, Z.; Guo, R.; Bhalla, A. S. *J. Appl. Phys. B* **2001**, *89*, 8085.
(43) Begg, B. D.; Finnie, K. S.; Vance, E. R. *J. Am. Ceram. Soc.* **1996**, *79*, 2666.
(44) Calos, N.; Forrester, J.; White, T. J.; Graves, P. R.; Myhra, S. *J. Mater. Sci.* **1995**, *30*, 4930.
(45) Perry, C. H.; Hall, D. B. *Phys. Rev. Lett.* **1965**, *15*, 700.
(46) Kanata, T.; Yoshikawa, T.; Kubota, K. *Solid State Commun.* **1987**, *62*, 765.
(47) Lobo, R. P. S. M.; Mohallem, N. D. S.; Moseira, R. L. *J. Am. Ceram. Soc.* **1995**, *78*, 1343.
(48) Gupta, S. *J. Raman Spectrosc.* **2002**, *33*, 42.
(49) Desu, S. B. *Phys. Status Solidi A* **1994**, *141*, 119.
(50) Akdogan, E. K.; Leonard, M. R.; Safari, A. In *Handbook of Low and High Dielectric Constant Materials and Their Applications*; Nalwa, H. S., Ed.; Academic Press: San Diego, CA, 1999; Vol. 2, p 62.
(51) Fatuzzo, E.; Merz, W. J. *Ferroelectricity*; North−Holland: Amsterdam, The Netherlands, 1967.
(52) Shaw, T. M.; Tralier-McKinstry, S.; McIntyre, P. C. *Annu. Rev. Mater. Sci.* **2000**, *30*, 263.
(53) Waser, R. *J. Am. Ceram. Soc.* **1988**, *71*, 58.
(54) Baikov, Yu. M.; Shalkova, E. K. *J. Solid State Chem.* **1992**, *97*, 224.
(55) Laulicht, I.; Benguigui, L. *Solid State Commun.* **1979**, *32*, 771.
(56) Kapphan, S.; Weber, G. *Ferroelectrics* **1981**, *37*, 673.
(57) Jovanovic, A.; Wöhlecke, M.; Kappan, S.; Mailard, A.; Godefroy, G. *J. Phys. Chem. Solids* **1989**, *50*, 632.
(58) Busca, G.; Buscaglia, V.; Leoni, M.; Nanni, P. *Chem. Mater.* **1994**, *6*, 955.
(59) Vivekanandan, R.; Kutty, T. R. N. *Powder Technol.* **1989**, *57*, 181.
(60) Spanier, J. E.; Kolpak, A. M.; Urban, J. J.; Grinberg, I.; Ouyang, L.; Yun, W. S.; Rappe, A. M.; Park, H. *Nano Lett.* **2006**, *6*, 735.